Polymers of Intrinsic Microporosity in the Design of Electrochemical Multicomponent and Multiphase Interfaces

Polymers of Intrinsic Microporosity (PIMs) in the Design of Electrochemical Multi-Component and Multi-Phase Interfaces

Frank Marken*[1], Mariolino Carta[2], Neil B. McKeown[3]

[1] Department of Chemistry, University of Bath, Claverton Down, Bath BA2 7AY, UK, email f.marken@bath.ac.uk; [2] Department of Chemistry, Swansea University, College of Science, Grove Building, Singleton Park, Swansea SA2 8PP, UK; [3] EaStCHEM, School of Chemistry, University of Edinburgh, Joseph Black Building, David Brewster Road, Edinburgh, Scotland EH9 3JF, UK

ABSTRACT: Polymers of Intrinsic Microporosity (or PIMs) provide porous materials due to their highly contorted and rigid macromolecular structures, which prevent space-efficient packing. PIMs are readily dissolved in solvents and can be cast into robust microporous coatings and membranes. With a typical micropore size range of around 1 nm and a typical surface area of 700-1000 m^2g^{-1}, PIMs offer channels for ion/molecular transport and pores for gaseous species, solids, and liquids to coexist. Electrode surfaces are readily modified with coatings or composite films to provide interfaces for solid|solid|liquid or solid|liquid|liquid or solid|liquid|gas multiphase electrode processes.

The concept of intrinsic microporosity for polymers emerged from work by Budd, McKeown, and coworkers in the early 2000s[1,2] and has been used in the design of materials for gas adsorption and gas separation. Intrinsic microporosity in PIM materials is causes by a highly rigid molecular backbone in the polymer leading to good solubility and poor packing in the solid. This leads to nanopores and channels with distinct interaction with different gases. However, more recently, the beneficial properties of polymers of intrinsic microporosity (PIMs) are finding a wider range of applications including in sensors, and as membranes for liquid phase separations and in electrochemistry.[3,4] In particular, there is increasing interest in the use of PIM membranes in connection with electrochemical energy storage[5,6] and redox flow cells.[7,8] The properties of PIMs depend on molecular weight, functional groups (e.g. to provide acidity/basicity), guest species, but also on the deposition method[9] and effects of aging[10] or exposure to air and light.[11] Molecular structures for prototypical types of PIMs considered in this article are shown in Figure 1.

PIMs as materials for ionic diodes. The PIM derived from ethanoanthracene (EA) and Tröger's base (TB) structural components, termed PIM-EA-TB, combines microporosity with well-defined basicity.

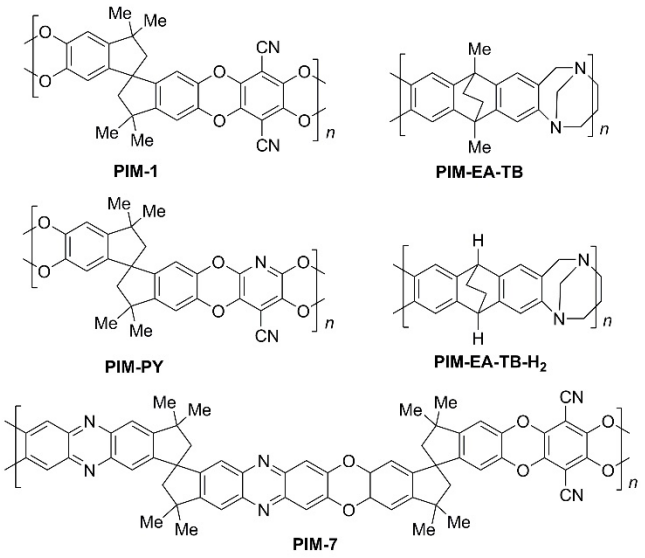

Figure 1. Molecular structures of some polymers of intrinsic microporosity (PIMs).

When employed as free-standing membrane, PIM-EA-TB has been shown to act as ion-conducting material, at pH >4, essentially conducting both cations and anions through its microporous structure. At low pH (< 4), protonation of the tertiary amines in the backbone (Figure 1) causes predominantly anion conductivity (protons remain immobile) inducing semi-permeability.[12]

The semi-permeability of PIM-EA-TB persists even for very thin films down to 300 nm thickness[13] and gives rise to ionic diode or ion current rectification effects as observed in four-

electrode membrane voltammetry experiments (see Figure 2). Due to the substrate, poly-(ethylene terephthalate) (PET) being asymmetrically coated with the PIM material[14] (Figure 2A), ion transport becomes partially uni-directional. Measurements are performed with the free-standing membrane situated between two electrolyte filled cells (see Figure 2A). By combining the asymmetric PIM-EA-TB coating with a complementary Nafion cation conductor coating, an asymmetric "heterojunction" interface is formed. The resulting cationic diode[15] (dominated by cation conduction and the semi-permeability of Nafion at neutral pH[16]) can be employed in the polymer|polymer interfacial precipitation of salts such as $KClO_4$, which can be considered as a potassium sensitive electroanalytical probe.[17] A sharp electrochemical response provides a tell-tale sign of high K^+ concentration at the interface (Figure 2C).

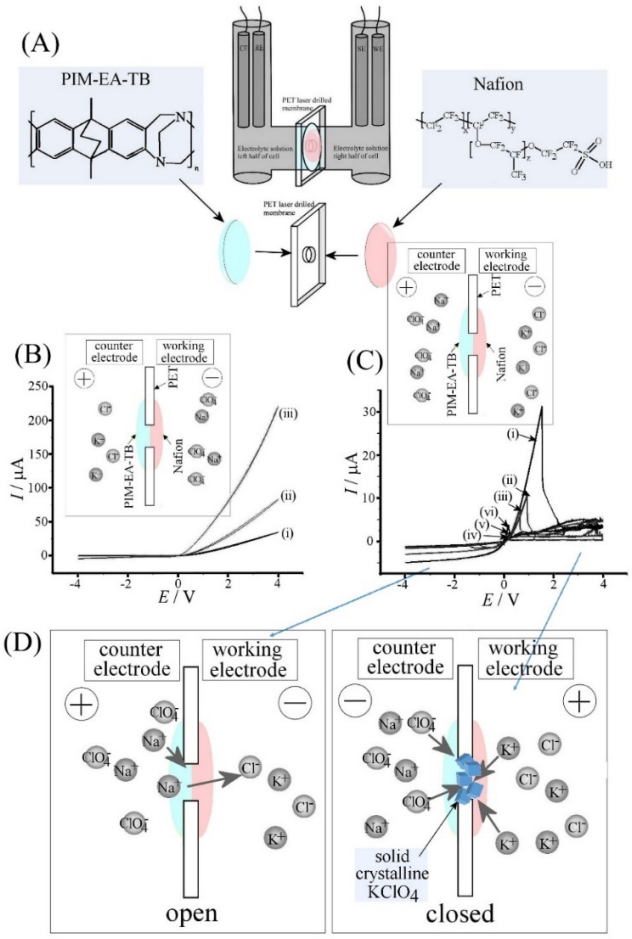

Figure 2. (A) Illustration of a four-electrode electrochemical cell to measure membrane properties for polymer coatings on a micro-hole in PET. (B) An ionic diode due to Nafion acting as cation semi-permeable film. (C) Inversion of the ionic diode due to K^+ and ClO_4^- precipitating at the polymer|polymer interface. (D) Schematic to explain the "open" and "closed" behaviour in (C) (Reproduced with permission from ref. 17. Copyright 2020 Publisher Elsevier).

Immobilisation of redox-active reagents within PIMs. When coated directly onto electrode surfaces, protonated PIM-EA-TB allows immobilisation of anions such as $PdCl_4^{2-}$, which can, in turn, be electrochemically reduced to Pd metal.[18] Protons bound to PIM-EA-TB as a function of pH can be detected directly at a platinum electrode.[19] This type of experiment confirmed that protonation of PIM-EA-TB occurs at ~pH 4. In addition, redox active anions, such as $Fe(CN)_6^{3-/4-}$, are readily immobilised into PIM-EA-TB to give redox active films. Hydrogen bonding interactions between $Fe(CN)_6^{3-/4-}$ and the protonated tertiary amine have been suggested to strongly contribute to the stability of these films, even when immersed in neutral aqueous environments.[20]

In addition to the absorption of redox active species, co-deposition of multi-component materials can also be employed to provide immobilisation, in particular for water-insoluble redox systems. For example, co-casting of tetraphenylporphyrinato-iron(II) complexes with PIM-EA-TB[21] gave microporous catalytically active films for oxygen reduction. Similarly, electrocatalytic saccharide[22] and alcohol oxidation processes were reported with 4-benzoyloxy-TEMPO as the water-insoluble molecular catalyst immobilised into PIM-EA-TB[23] (Figure 3). A thin film of PIM-EA-TB with glassy carbon spheres allowed the active surface area to be increased and a range of substrates including aliphatic alcohols, glucose, and benzylalcohol were investigated. More hydrophobic alcohols were shown to be associated with higher catalytic currents, which led to the hypothesis of hydrophobicity promoting preferential alcohol partitioning into the PIM-EA-TB embedded catalyst film.

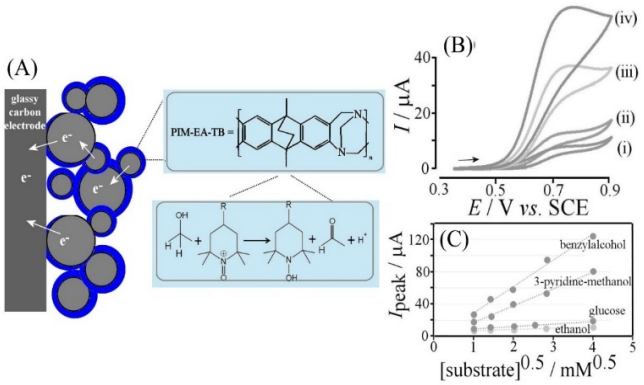

Figure 3. (A) Schematic of the glassy carbon electrode with carbon spheres (to increase surface area) and PIM-EA-TB containing 4-benzoyloxy-TEMPO. (B) Cyclic voltammograms (C) Plot of the current peak versus square root of substrate concentration (Reproduced with permission from ref. 23. Copyright 2020 Publisher Springer).

PIMs at solid|solid|liquid interfaces. Composites of PIM materials with solid guest species are readily formed by solution casting. It was shown that graphene oxide can be embedded into a film of PIM-1.[24] When embedding praseodymium nitrite into PIM-EA-TB followed by calcination, nanofibrous Pr_6O_{11} was obtained as a solid product after removal of the polymer template.[25]

Solid catalyst nanoparticles can be embedded into the PIM materials without loss of catalyst activity. During the growth of platinum nanoparticles in solution, PIM-EA-TB can be employed as a non-surface-blocking capping agent, in which platinum nanoparticles are protected from aggregation and precipitation (the platinum-to-polymer binding is likely due to interfacial Pt-N interactions[26]). The resulting stable colloidal solutions

can be deposited and converted into PIM-catalyst composite films. When coated onto electrode surfaces, these capped platinum nanoparticles (of diameter 3.1 to 4.2 nm) give catalytically active and electrically conducting films with lower polymer content and electrically insulating films for higher polymer content (*i.e.* beyond the percolation threshold). Beneficial effects due to platinum nanoparticle capping were also observed when PIM-EA-TB was coated directly over classic Vulcan-Pt(40%) fuel cell nanocatalysts.[27,28] Accelerated corrosion testing by potential cycling was shown to strongly affect bare Vulcan-Pt(40%) but not the PIM-EA-TB coated catalyst. Catalytic performance for methanol and ethanol oxidation in the presence of the PIM-EA-TB polymer coating was not impeded, but degradation due to dislodged catalyst or carbon nanoparticles was inhibited.

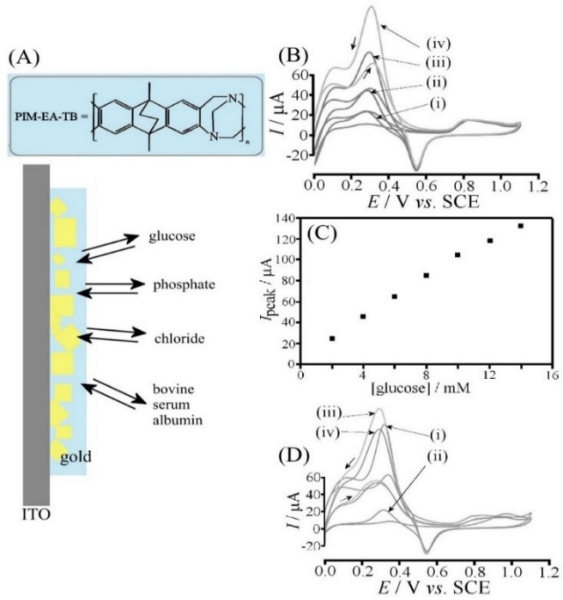

Figure 4. (A) Schematic showing gold nanoparticles electrodeposited onto tin-doped indium oxide (ITO) and coated with PIM-EA-TB. (B) Cyclic voltammograms (scan rate 5 mVs^{-1}, start point 0.0 V vs. SCE) for the oxidation of (i) 2, (ii) 4, (iii) 8, (iv) 14 mM glucose at gold nanoparticle on ITO, coated with 500 nm PIM-EA-TB, and immersed in 0.1 M phosphate buffer pH 7. (C) Plot of the peak current for glucose oxidation versus glucose concentration. (D) Cyclic voltammograms (scan rate 5 mVs^{-1}) for the oxidation of 14 mM glucose at gold nanoparticle on ITO immersed in 0.1 M phosphate buffer pH 7 (i) without and (ii) with BSA (3 mg in 50 cm^{-3} solution) and the same experiment with PIM-EA-TB coating (iii) without and (iv) with BSA (Reproduced with permission from ref. 30. Copyright 2020 Publisher John Wiley & Sons).

In related work, silver microparticles coated with PIM-EA-TB[29] and gold nanoparticles coated with PIM-EA-TB[30] were studied. Gold nanoparticles grown electrolytically in the presence of sulphate allow glucose oxidation in aqueous phosphate buffer media at pH 7 (see Figure 4). The PIM-EA-TB coating was shown to stop catalyst poisoning by bigger proteins such as bovine serum albumin. However, the PIM-EA-TB coating did not prevent the competition of glucose binding and phosphate binding and/or chloride catalyst poisoning. Figure 4B shows data for the oxidation of glucose in 0.1 M phosphate buffer at pH 7. Figure 4C shows a plot for the catalytic current peak (observed in the presence of PIM-EA-TB coating) *versus* glucose concentration. Figure 4D demonstrates the effect of bovine serum albumin (BSA) on electrodes that are not protected by the PIM-EA-TB coating.

Due to their molecularly rigid backbone, PIM materials show interesting behaviour when heated up to thermolysis/carbonisation conditions. For PIM-EA-TB and for PIM-EA-TB-H_2[31] it has been reported that the total volume and shape of the polymer remain constant. This could be due to the backbone/packing remaining intact and molecular fragmentation only resulting in some cross-linking. For the formation of an electrically conducting heterocarbon, the observed Brunauer-Emmett-Teller (BET) surface area decreased from 1027 m^2g^{-1} to 242 m^2g^{-1}, but the cumulative pore volume remained close to constant at 1.6 cm^3g^{-1}. The resulting carbon materials contain nitrogen and show electrical conductivity and electrochemical capacitor properties.[32] This method of carbonisation can be used also for PIMs with absorbed metal complexes, for example for absorbed $PtCl_6^{2-}$ to embed platinum nanoparticles into the microporous carbon product.[33] In recent work by Jeon *et al*. with PIM-EA-TB, it was shown that non-solvent precipitation methods can be employed to add hierarchical porosity for electrochemical supercapacitor applications.[34]

PIMs at solid|liquid|liquid interfaces. Organogel systems are of interest in processes that require mechanically stable liquid|liquid interfaces[35] and for the immobilisation of liquid materials onto electrode surfaces.[36] Microporous polymers can be employed to immobilise a water immiscible organic phase on the electrode surface.

The formation of an organogel coating was demonstrated for PIM-EA-TB with (3-phenylpropyl)-pyridine.[37] Two redox active metal complexes, tetraphenyl-porphyrinato-Mn(III/II) (MnTPP) and phthalocyanato-Mn(III/II) (MnPc), were dissolved in the organic phase and investigated by cyclic voltammetry and *in situ* spectroelectrochemistry. Figure 5B shows UV/Vis spectroscopy data as a function of applied potential with prominent absorption bands for MnTPP switching as a function of redox state. Due to the need for anion exchange during redox switching, the nature of the electrolyte anion contributes to the appearance of the voltammetric responses. More hydrophobic anions such as PF_6^- shift the midpoint potential for electron/ion transfer to more negative potentials. Figure 5D shows a plot of midpoint potential for both MnTPP and MnPc in the organogel for a range of anions. For highly hydrophilic anions such as fluoride and sulphate a change in mechanism occurs probably due to preferential transfer of hydroxide. Coupling of anion transfer with electron transfer and further chemical reaction steps were observed.

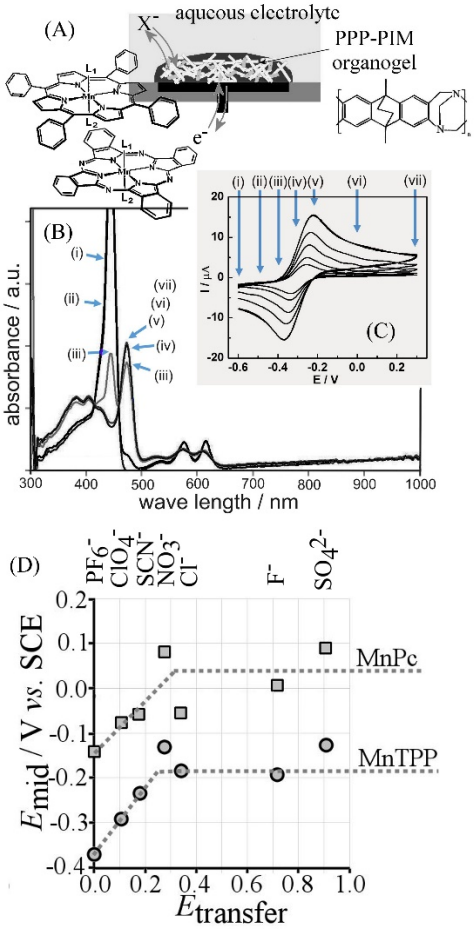

Figure 5. (A) Molecular structures for a PIM-EA-TB, MnTPP, MnPc, and schematic drawing of an organogel deposit composed of 4-(3-phenylpropyl)-pyridine (PPP) with PIM-EA-TB and a redox active Mn(II) complex in a coupled electron transfer with liquid/liquid anion transfer. (B) Spectroelectrochemical data (at selected applied potentials) for a MnTPP/PIM-EA-TB/PPP organogel immobilized onto porous ITO and immersed into aqueous 0.1 M $NaClO_4$. (C) Cyclic voltammograms (scan rate 10, 20, 50, 100, 200 mV s^{-1}) for a deposit of MnTPP/PIM-EA-TB/PPP organogel on a 3 mm diameter glassy carbon electrode immersed into aqueous 0.1 M $NaClO_4$ electrolyte media. (D) Plot of midpoint potentials *versus* anion transfer potential for MnPc and MnTPP in 0.1 M electrolyte media (Reproduced with permission from ref. 37. Copyright 2020 Publisher Springer).

PIMs at solid|liquid|gas interfaces. The solid|liquid|gas multi-phase electrode system is technically important for gas evolution reaction and gas consuming reactions. For example, recent reports on the formation of a microporous carbon mat from electrospun PIM-1 suggested that application in gas diffusion electrodes are possible.[38,39]

PIM materials have been shown to affect the way gases interact with the electrode or catalyst surface.[40] Both PIM-1 and PIM-PY (Figure 1) were observed to bind gaseous species such as hydrogen and oxygen when immersed in aqueous electrolyte.[41] Figure 6 shows data from cyclic voltammetry with a platinum disk electrode immersed in 0.01 M phosphate buffer pH 7.7 solution. Trace (i) is for the base electrode and trace (ii) is for the electrode coated with PIM-1. In the presence of the polymer, the characteristic platinum current peaks are partially suppressed but still identifiable. The typical hydrogen adsorption peaks on platinum (denoted Process 1 and Process 2 associated with different facets of crystalline platinum;[42]) occur at -0.38 V vs. SCE and at -0.48 V vs. SCE.

Process 1: $H^+(aq) + e^-(Pt) \rightleftharpoons$ Pt-H(strong)
Process 2: $H^+(aq) + e^-(Pt) \rightleftharpoons$ Pt-H(weak)

When scanning the applied potential into the more negative range (Figure 6B trace i), an additional reduction peak is detected associated with hydrogen evolution and with consumption of protons from the buffer system (consuming protons from $H_2PO_4^-(aq)$; Process 3). In the presence of the PIM-1 coating this current response also is suppressed (Figure 6B trace ii). However, during the re-oxidation of hydrogen more current is observed and a new current peak assigned to hydrogen trapped in the PIM-1 (Process 4).

Process 3: $2\ H^+(aq) + 2\ e^- \rightleftharpoons H_2(g)$
Process 4: $2\ H^+(aq) + 2\ e^- \rightleftharpoons H_2(aq) \rightleftharpoons H_2(PIM)$

In consecutive potential cycles Process 4 can be seen to further develop (Figure 6C). For PIM-1 coated onto glassy carbon, an effect on oxygen reduction is observed (Figure 6D). This process is known to be dominated by the two-electron reduction of oxygen to hydrogen peroxide (Process 5). Trace (i) shows a single peak for this oxygen reduction process at a bare electrode. Trace (ii) and (iii) show data for PIM-1 and PIM-PY, respectively, coated onto the glassy carbon. In both cases a catalytic pre-peak is observed consistent with the binding of ambient oxygen into the PIM-1 or PIM-PY material to enhance the local oxygen activity (Figure 6, inset).

Process 5: $O_2(aq) + 2\ H^+(aq) + 2\ e^- \rightleftharpoons H_2O_2$
Process 6: $O_2(PIM) + 2\ H^+(aq) + 2\ e^- \rightleftharpoons H_2O_2$

Mechanistic details for this shift in oxygen reduction potential and aspects of the molecular polymer structure controlling the oxygen reduction mechanism are not fully resolved, but additional rotating ring-disk electrode experiments have been reported confirming the observation and the presence of the enhanced oxygen reduction under hydrodynamic steady state conditions. Therefore, both hydrogen binding and oxygen binding onto the microporous polymers occurs in a way that electrode processes are modified. Under these conditions gaseous, liquid, and solid phase co-exist in a triphasic system, but the nature and distribution of gaseous species in micropores will need further investigation.

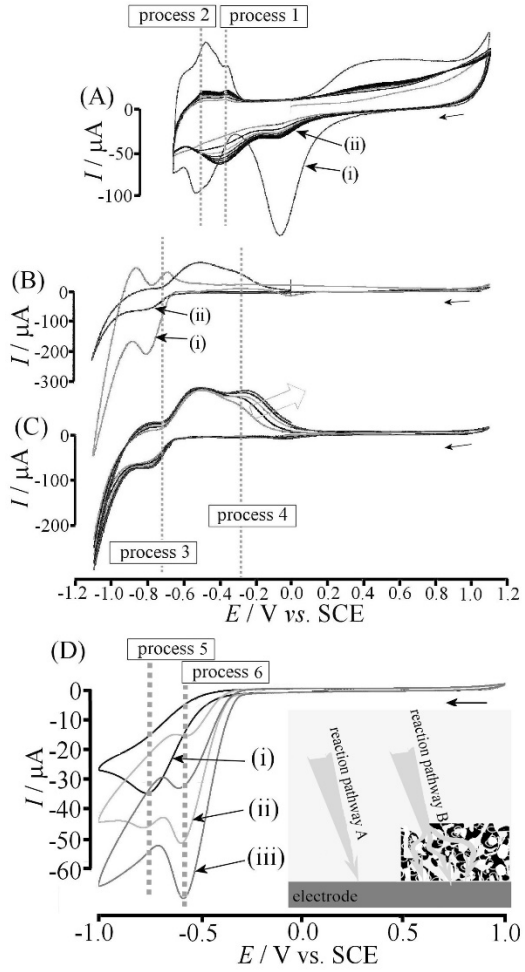

Figure 6. (A) Cyclic voltammograms (scan rate 50 mVs^{-1}; 3 mm diameter electrodes) for a Pt disk electrode immersed in 0.01 M phosphate buffer pH 7.7 for (i) the bare electrode and (ii) a 20 µg PIM-1 nanoparticle deposit. (B) As before for scan rate 50 mVs^{-1} and (i) bare platinum and (ii) 20 µg PIM-1 nanoparticle deposit. (C) As before but for five consecutive potential cycles. (D) Cyclic voltammograms for the reduction of ambient oxygen in aqueous 0.01 M phosphate buffer solution at pH 7 for (i) a bare glassy carbon, (ii) 20 µg nanoparticulate PIM-1 on glassy carbon, (iii) 20 µg nanoparticulate PIM-PY on glassy carbon (reproduced with permission). Inset shows an illustration of the multiphase coating (Reproduced with permission from ref. 41. Copyright 2020 Publisher John Wiley & Sons).

In a related study, the effect of PIM-7 coatings on palladium electrocatalyst were investigated.[43] Palladium nanoparticles were formed on a glassy carbon surface and the catalyst was coated with PIM-7. Processes such as hydroquinone oxidation or methanol oxidation were observed to remain unaffected or only slightly suppressed by the PIM-7 polymer coating. However, the oxidation of formic acid was enhanced, particularly for higher concentrations of formic acid. The oxidation of formic acid appeared to be associated with the spontaneous formation of hydrogen gas, which was "stored" in the PIM-7 coating and therefore more accessible in a multiphase film coating rather than gas bubbles partially blocking the catalyst surface.

PIM-EA-TB when protonated can bind $PdCl_4^{2-}$ anions into micropores. Carbonisation under vacuum thermolysis conditions has been shown to yield flakes of microporous carbon with embedded Pd nanoparticles that are 10 nm to 30 nm in diameter.[44] The microporous nature of this Pd-carbon composite allows only small redox active molecules to access the catalyst, so that in a solution of aqueous formic acid and ambient oxygen only oxygen reduction occurs. This is in contrast to bare palladium where formic acid is oxidised. When combined these two types of electrodes immersed in the same solution provide a membrane-less micro-power source: spontaneous formic acid oxidation occurs at palladium and spontaneous oxygen reduction occurs at Pd@cPIM.

A similar effect was noted with a composite catalyst material derived from PIM-EA-TB-H_2 (Figure 7). Protonation and absorption of $PtCl_6^{2-}$ followed by vacuum thermolysis gave a microporous carbon catalyst material with embedded platinum nanoparticles of typically 1 to 3 nm diameter.[45] This material could be employed in catalysis without any pre-activation due to some degree of microporosity being maintained. This catalyst was tested for the production of H_2O_2 directly from a mixture of hydrogen and oxygen gas. This reaction is suggested to be associated with rapid hydrogen diffusion into the composite catalyst where reaction on platinum provides electrons and protons. The electrons migrate out and oxygen reduction to hydrogen peroxide occurs on the outside of the catalyst particles (see illustration in Figure 7).

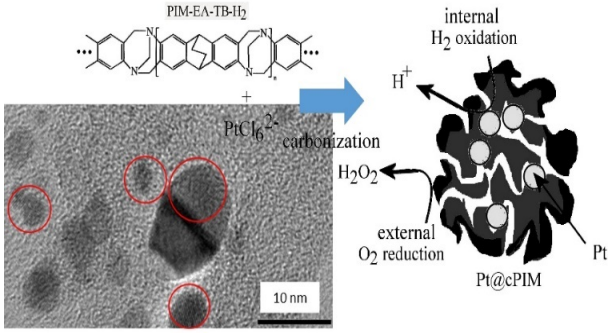

Figure 7. Molecular structure of PIM-EA-TB-H_2 and typical TEM micrograph for Pt nanoparticles formed in the resulting carbonised matrix. When employed in catalytic reactions of hydrogen and oxygen to hydrogen peroxide, the hydrogen is suggested to permeate into the micropores to react with platinum whereas oxygen only reacts externally on the carbon to form H_2O_2 (see illustration; Reproduced with permission from ref. 45. Copyright 2020 Publisher MDPI).

Gaseous species and reaction intermediates are important also in photoelectrochemical multiphase processes. For example, a composite film of PIM-1 and Pt@titanate nanosheets, when deposited onto either glassy carbon or platinum disk electrodes, demonstrates ambient oxygen reduction in the dark. However, when illuminated with 385 nm LED light, the oxygen reduction signal was suppressed. Photo-current transients produced with pulsed LED light were shown to give a quantitative correlation to oxygen concentration. The mechanism has been discussed in terms of photoelectrochemical oxygen reduction being coupled to PIM-1 photooxidation.[46] The role of PIM-1 in

this process was not fully resolved and may be more than that of a quencher or an innocent microporous scaffold, as recent work suggests that photoexcited PIM-1 is able to generate singlet oxygen within its microporous structure.[47]

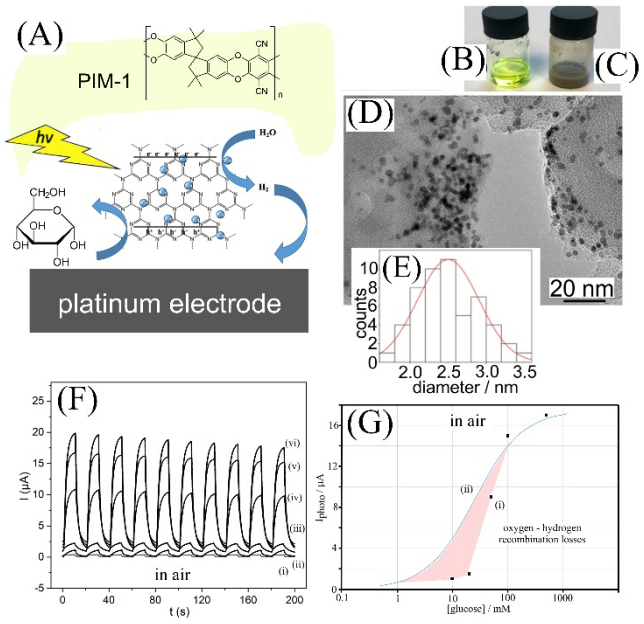

Figure 8. (A) Illustration of Pt@g-C_3N_4 photocatalyst at a platinum electrode surface generating hydrogen. A PIM-1 coating is applied to provide mechanical stability, to capture hydrogen, and to provide triphasic reaction conditions. Photographic images of (B) PIM-1 solution in chloroform and (C) of the Pt@g-C_3N_4 suspension in isopropanol. (D) Characterisation of Pt@g-C_3N_4 with TEM. (E) Histogram of the platinum nanoparticle size distribution with a maximum at diameter 2.5 nm. (F) Chronoamperometry data (0.0 V vs. SCE; 10 s on and 10 s off, 385 nm LED) at a 3 mm diameter platinum disk electrode coated with Pt@g-C_3N_4 with 30 µg PIM-1 and immersed in 0.1M NaOH with (i) 0.0, (ii) 10, (iii) 20, (iv) 50, (v) 100, and (vi) 500 mM glucose in ambient air with 75 µg Pt@g-C_3N_4. (G) Plot of photocurrent versus glucose concentration with a line indicating the Langmuir model with binding constant 40 $mol^{-1}dm^3$ (Reproduced with permission from ref. 49. Copyright 2020 Publisher Elsevier).

A coating of PIM-1 was employed on photocatalyst Pt@g-C_3N_4, which is based on the organic photocatalyst graphitic carbon nitride[48] (with platinum nanoparticles decorated onto the surface; see Figure 8), that is able to generate holes and electrons during photo-excitation. Saccharides such as glucose can be used as hole quenchers to leave electrons to generate hydrogen gas from water.[49] The effect of glucose concentration on photocurrents suggests a clear interfacial adsorption effect with a switch in behaviour from low concentration to high concentration (Figure 8G). Films of Pt@g-C_3N_4 on a platinum disk electrode produce hydrogen, which is then transported to the platinum substrate to generate protons and electrons and a negative potential. PIM-1 coatings were found to mechanically stabilise this particulate catalyst-electrode assembly and to help guide the hydrogen to the electrode surface. Similar results were reported in "indirect photoelectrochemical processes"[50] in which Pt@g-C_3N_4 and PIM-1 were coated onto a thin palladium film. In this system, the production of hydrogen (in the presence of glucose, fructose, sucrose, or trehalose) occurs in a catalysis compartment independent of the electrochemical compartment. Photochemical hydrogen generation was linked to hydrogen permeating through the thin palladium film to then give electricity on the opposite side of the membrane in the electrochemical compartment. The system provided an electroanalytical potential reading that correlated approximately to the total carbohydrate content for example in a commercial soft drink.

Summary and Outlook. PIMs offer new opportunities for interfacial design for electrodes and sensor surfaces with free-standing membranes, films, and coatings being readily produced from polymer solutions in organic solvents (*e.g.* in tetrahydrofuran or chloroform). Although only very few types of PIM have been studied so far (and without any optimisation of the molecular structures), there appear to be a wide range of potential applications emerging in electrochemistry and in electroanalysis. In addition, for electrochemical energy storage in lithium batteries, PIM membranes offer alternatives to classic separator materials leading to suppression of metal dendrites.[51,52] For redox flow batteries PIMs provide high cation permeability and suppression of cross-over of redox active molecules.[53,54,55] As shown in this article, for electroanalytical applications, PIMs offer size selectivity and partitioning effects for accumulation of analytes. When studied as film deposits on electrodes, PIM materials provide catalyst coatings as mechanical support, as a way to suppress deterioration, and as a way to introduce size-selectivity for smaller redox species. When treated at high temperature, PIMs provide access to new microporous heterocarbon materials with/without embedded catalysts formed in one step. Embedded catalysts remain active due to inability of the rigid PIM backbone to interact/block the surface.

For multiphase electrochemical systems, PIMs provide control over interfacial processes, such as reactions involving immobilised solids or catalysts, processes in immobilised water-immiscible liquids containing redox actives species, and reactions involving gaseous redox species interacting with electrodes and catalysts. Gas bubble formation on the surface of catalysts can be suppressed and gaseous products/intermediates can be captured in hydrophobic microporous materials such as PIM-1 or PIM-7. In the future, a much greater structural diversity of PIMs could provide a toolbox of materials to electrochemists and engineers to develop processes in electrochemical energy technology, electrosynthesis, and in electroanalysis.

ACKNOWLEDGMENT

The authors are grateful for support from the Leverhulme Foundation (RPG2014-308: "New Materials for Ionic Diodes and Ionic Photodiodes").

AUTHOR BIOGRAPHIES

Frank Marken (Dr. rer. nat.) worked as a Stipendiary Lecturer at the University of Oxford (UK) before moving to the University of Loughborough (UK) in 2000. In September 2004, he was appointed

to a Senior Lecturer position at the University of Bath (UK), and in 2011 promoted to a personal chair in Physical Chemistry.

Mariolino Carta completed his PhD in Organic Material Chemistry at Cardiff University (UK) in 2008. He then held positions at Cardiff University until 2014 and at the University of Edinburgh (UK). In October 2017, he was appointed as Lecturer in Chemistry at Swansea University (UK).

Neil B. McKeown (PhD) is the Crawford Tercentenary Chair of Chemistry at The University of Edinburgh (UK). His research involves using organic chemistry to develop novel porous materials, both crystalline and amorphous, for use in molecular separations, catalysis and sensors.

REFERENCES

(1) Budd, P.M.; Ghanem, B.S.; Makhseed, S.; McKeown, N.B.; Msayib, K.J.; Tattershall, C.E. Polymers of Intrinsic Microporosity (PIMs): Robust, Solution-Processable, Organic Nanoporous Materials. *Chem. Commun.* **2004**, 230–231.

(2) Low, Z.X.; Budd, P.M.; McKeown, N.B.; Patterson, D.A. Gas Permeation Properties, Physical Aging, and Its Mitigation in High Free Volume Glassy Polymers. *Chem. Rev*. **2018**, *118*, 5871–5911.

(3) Madrid, E.; McKeown, N.B. Innovative Methods in Electrochemistry Based on Polymers of Intrinsic Microporosity. Curr. Opinion Electrochem. 2018, 10, 61–66.

(4) Wang, L.N.; Zhao, Y.Z.; Fan, B.B.; Carta, M.; Malpass-Evans, R.; McKeown, N.B.; Marken, F. Polymer of Intrinsic Microporosity (PIM) Films and Membranes in Electrochemical Energy Storage and Conversion: A Mini-Review. *Electrochem. Commun.* **2020**, *118*, 106798.

(5) Doris, S.E.; Ward, A.L.; Frischmann, P.D.; Li, L.J.; Helms, B.A. Understanding and Controlling the Chemical Evolution and Polysulfide-Blocking Ability of Lithium-Sulfur Battery Membranes Cast from Polymers of Intrinsic Microporosity. *J. Mater. Chem. A* **2016**, *4*, 16946–16952.

(6) Yang, Q.L.; Li, W.L.; Dong, C.; Ma, Y.Y.; Yin, Y.X.; Wu, Q.B.; Xu, Z.T.; Ma, W.; Fan, C.; Sun, K.N. PIM-1 as an Artificial Solid Electrolyte Interphase for Stable Lithium Metal Anode in High-Performance Batteries. *J. Energy Chem*. **2020**, *42*, 83–90.

(7) Baran, M.J.; Braten, M.N.; Sahu, S.; Baskin, A.; Meckler, S.M.; Li, L.J.; Maserati, L.; Carrington, M.E.; Chiang, Y.M.; Prendergast, D.; Helms, B.A. Design Rules for Membranes from Polymers of Intrinsic Microporosity for Crossover-free Aqueous Electrochemical Devices. Joule 2019, 3, 2968–2985.

(8) Chae, I.; Luo, T.; Moon, G.H.; Ogieglo, W.; Kang, Y.S.; Wessling, M. Ultra-High Proton/Vanadium Selectivity for Hydrophobic Polymer Membranes with Intrinsic Nanopores for Redox Flow Battery. *Adv. Energy Mater*. **2016**, *6*, 1600517.

(9) Bernardo, P.; Scorzafave, V.; Clarizia, G.; Tocci, E.; Jansen, J.C.; Borgogno, A.; Malpass-Evans, R.; McKeown, N.B.; Carta, M.; Tasselli, F. Thin Film Composite Membranes Based on a Polymer of Intrinsic Microporosity Derived from Tröger's Base: A Combined Experimental and Computational Investigation of the Role of Residual Casting Solvent. *J. Membrane Sci.* **2019**, *569*, 17–31.

(10) Lau, C.H.; Konstas, K.; Doherty, C.M.; Smith, S.J.D.; Hou, R.J.; Wang, H.T.; Carta, M.; Yoon, H.; Park, J.; Freeman, B.D.; Malpass-Evans, R.; Lasseuguette, E.; Ferrari, M.C.; McKeown, N.B.; Hill, M.R. Tailoring Molecular Interactions between Microporous Polymers in High Performance Mixed Matrix Membranes for Gas Separations. *Nanoscale* **2020**, *12*, 17405–17410.

(11) Song, Q.L.; Cao, S.; Zavala-Rivera, P.; Lu, L.P.; Li, W.; Ji, Y.; Al-Muhtaseb, S.A.; Cheetham, A.K.; Sivaniah, E. Photo-oxidative Enhancement of Polymeric Molecular Sieve Membranes. *Nature Commun.* **2013**, *4*, 1918.

(12) Madrid, E.; Rong, Y.Y.; Carta, M.; McKeown, N.B.; Malpass-Evans, R.; Attard, G.A.; Clarke, T.J.; Taylor, S.H.; Long, Y.T.; Marken, F. Metastable Ionic Diodes Derived from an Amine-Based Polymer of Intrinsic Microporosity. *Angew. Chem. Inter. Ed*. **2014**, *53*, 10751–10754.

(13) Rong, Y.Y.; Song, Q.L.; Mathwig, K.; Madrid, E.; He, D.P.; Niemann, R.G.; Cameron, P.J.; Dale, S.E.C.; Bending, S.; Carta, M.; Malpass-Evans, R.; McKeown, N.B.; Marken, F. PH-induced Reversal of Ionic Diode Polarity in 300 nm Thin Membranes Based on a Polymer of Intrinsic Microporosity. *Electrochem. Commun.* **2016**, *69*, 41–45.

(14) Mathwig, K.; Aaronson, B.D.B.; Marken, F. Ionic Transport in Microhole Fluidic Diodes Based on Asymmetric Ionomer Film Deposits. *ChemElectroChem* **2018**, *5*, 897–901.

(15) Putra, B.R.; Aaronson, B.D.B.; Madrid, E.; Mathwig, K.; Carta, M.; Malpass-Evans, R.; McKeown, N.B.; Marken, F. Ionic Diode Characteristics at a Polymer of Intrinsic Microporosity (PIM) | Nafion "Heterojunction" Deposit on a Microhole Poly(ethylene-terephthalate) Substrate. *Electroanalysis* **2017**, *29*, 2217–2223.

(16) He, D.P.; Madrid, E.; Aaronson, B.D.B.; Fan, L.; Doughty, J.; Mathwig, K.; Bond, A.M.; McKeown, N.B.; Marken, F. A Cationic Diode Based on Asymmetric Nafion Film Deposits. *ACS Appl. Mater. Interfaces* **2017**, *9*, 11272–11278.

(17) Putra, B.R.; Carta, M.; Malpass-Evans, R.; McKeown, N.B.; Marken, F. Potassium Cation Induced Ionic Diode Blocking for a Polymer of Intrinsic Microporosity | Nafion "Heterojunction" on a Microhole Substrate. *Electrochim. Acta* **2017**, *258*, 807–813.

(18) Xia, F.J.; Pan, M.; Mu, S.C.; Malpass-Evans, R.; Carta, M.; McKeown, N.B.; Attard, G.A.; Brew, A.; Morgan, D.J.; Marken, F. Polymers of Intrinsic Microporosity in Electrocatalysis: Novel Pore Rigidity Effects and Lamella Palladium Growth. *Electrochim. Acta* **2014**, *128*, 3–9.

(19) Rong, Y.Y.; Kolodziej, A.; Madrid, E.; Carta, M.; Malpass-Evans, R.; McKeown, N.B.; Marken, F. Polymers of Intrinsic Microporosity in Electrochemistry: Anion Uptake and Transport Effects in Thin Film Electrodes and in Free-standing Ionic Diode Membranes. *J. Electroanal. Chem*. **2016**, *779*, 241–249.

(20) Wang, L.N.; Malpass-Evans, R.; Carta, M.; McKeown, N.B.; Marken, F. The Immobilisation and Reactivity of $Fe(CN)_6^{3-/4-}$ in an Intrinsically Microporous Polyamine (PIM-EA-TB). *J. Solid State Electrochem.* **2020**, https://doi.org/10.1007/s10008-020-04603-4.

(21) Rong, Y.Y.; Malpass-Evans, R.; Carta, M.; McKeown, N.B.; Attard, G.A.; Marken, F. High Density Heterogenisation of Molecular Electrocatalysts in a Rigid Intrinsically Microporous Polymer. *Electrochem. Commun.* **2014**, *46*, 26–29.

(22) Kolodziej, A.; Ahn, S.D.; Carta, M.; Malpass-Evans, R.; McKeown, N.B.; Chapman, R.S.L.; Bull, S.D.; Marken, F. Electrocatalytic Carbohydrate Oxidation with 4-Benzoyloxy-TEMPO Heterogenised in

a Polymer of Intrinsic Microporosity. *Electrochim. Acta* **2015**, *160*, 195–201.

(23) Ahn, S.D.; Kolodziej, A.; Malpass-Evans, R.; Carta, M.; McKeown, N.B.; Bull, S.D.; Buchard, A.; Marken, F. Polymer of Intrinsic Microporosity Induces Host-Guest Substrate Selectivity in Heterogeneous 4-Benzoyloxy-TEMPO-Catalysed Alcohol Oxidations. *Electrocatalysis* **2016**, *7*, 70–78.

(24) Rong, Y.Y.; Large, M.J.; Tripathi, M.; Ogilvie, S.P.; Graf, A.A.; Mao, B.Y.; Tunesi, J.; Salvage, J.P.; King, A.A.K.; Pasquazi, A.; Peccianti, M.; Malpass-Evans, R.; McKeown, N.B.; Marken, F.; Dalton, A.B. Charge Transfer Hybrids of Graphene Oxide and the Intrinsically Microporous Polymer PIM-1. *ACS Appl. Mater. Interfaces* **2019**, *11*, 31191–31199.

(25) Al-Kutubi, H.; Rassaei, L.; Olthuis, W.; Nelson, G.W.; Foord, J.S.; Holdway, P.; Carta, M.; Malpass-Evans, R.; McKeown, N.B.; Tsang, S.C.; Castaing, R.; Forder, T.R.; Jones, M.D.; He, D.; Marken, F. Polymers of Intrinsic Microporosity as High Temperature Templates for the Formation of Nanofibrous Oxides. *RSC Adv.* **2015**, *5*, 73323–73326.

(26) He, D.P.; He, D.S.; Yang, J.L.; Low, Z.X.; Malpass-Evans, R.; Carta, M.; McKeown, N.B.; Marken, F. Molecularly Rigid Microporous Polyamine Captures and Stabilizes Conducting Platinum Nanoparticle Networks. *ACS Appl. Mater. Interfaces* **2016**, *8*, 22425–22430.

(27) He, D.P.; Rong, Y.Y.; Kou, Z.K.; Mu, S.C.; Peng, T.; Malpass-Evans, R.; Carta, M.; McKeown, N.B.; Marken, F. Intrinsically Microporous Polymer Slows Down Fuel Cell Catalyst Corrosion. *Electrochem. Commun.* **2015**, *59*, 72–76.

(28) He, D.P.; Rong, Y.Y.; Carta, M.; Malpass-Evans, R.; McKeown, N.B.; Marken, F. Fuel Cell Anode Catalyst Performance can be Stabilized with a Molecularly Rigid Film of Polymers of Intrinsic Microporosity (PIM). *RSC Adv*. **2016**, *6*, 9315–9319.

(29) He, D.P.; Rauwel, E.; Malpass-Evans, R.; Carta, M.; McKeown, N.B.; Gorle, D.B.; Kulandainathan, M.A.; Marken, F. Redox Reactivity at Silver Microparticle-Glassy Carbon Contacts under a Coating of Polymer of Intrinsic Microporosity (PIM). *J. Solid State Electrochem.* **2017**, *21*, 2141–2146.

(30) Rong, Y.Y.; Malpass-Evans, R.; Carta, M.; McKeown, N.B.; Attard, G.A.; Marken, F. Intrinsically Porous Polymer Protects Catalytic Gold Particles for Enzymeless Glucose Oxidation. *Electroanalysis* **2014**, *26*, 904–909.

(31) Hernandez, N.; Iniesta, J.; Leguey, V.M.; Armstrong, R.; Taylor, S.H.; Madrid, E.; Rong, Y.Y.; Castaing, R.; Malpass-Evans, R.; Carta, M.; McKeown, N.B.; Marken, F. Carbonization of Polymers of Intrinsic Microporosity to Microporous Heterocarbon: Capacitive pH Measurements. *Appl. Mater. Today,* **2017**, *9*, 136–144.

(32) Rong, Y.Y.; He, D.P.; Sanchez-Fernandez, A.; Evans, C.; Edler, K.J.; Malpass-Evans, R.; Carta, M.; McKeown, N.B.; Clarke, T.J.; Taylor, S.H.; Wain, A.J.; Mitchels, J.M.; Marken, F. Intrinsically Microporous Polymer Retains Porosity in Vacuum Thermolysis to Electroactive Heterocarbon. *Langmuir* **2015**, *31*, 12300–12306.

(33) Rong, Y.Y.; He, D.P.; Malpass-Evans, R.; Carta, M.; McKeown, N.B.; Gromboni, M.F.; Mascaro, L.H.; Nelson, G.W.; Foord, J.S.; Holdway, P.; Dale, S.E.C.; Bending, S.; Marken, F. High-Utilisation Nanoplatinum Catalyst (Pt@cPIM) Obtained via Vacuum Carbonisation in a Molecularly Rigid Polymer of Intrinsic Microporosity. *Electrocatalysis* **2017**, *8*, 132–143.

(34) Jeon, J.W.; Shin, J.; Lee, J.; Baik, J.H.; Malpass-Evans, R.; McKeown, N.B.; Kim, T.H.; Lee, J.C.; Kim, S.K.; Kim, B.G. Hierarchically Structured Carbon Electrodes Derived from Intrinsically Microporous Tröger's Base Polymers for High-Performance Supercapacitors. *Appl. Surface Sci.* **2020**, *530*, 147146.

(35) Booth, S.G.; Felisilda, B.M.B.; de Eulate, E.A.; Gustafsson, O.J.R.; Arooj, M.; Mancera, R.L.; Dryfe, R.A.W.; Hackett, M.J.; Arrigan, D.W.M. Damien Secondary Structural Changes in Proteins as a Result of Electroadsorption at Aqueous-Organogel Interfaces. *Langmuir* **2019**, *35*, 5821–5829.

(36) Marken, F.; Watkins, J.D.; Collins, A.M. Ion-Transfer- and Photo-Electrochemistry at Liquid | Liquid | Solid Electrode Triple Phase Boundary Junctions: Perspectives. *Phys. Chem. Chem. Phys.* **2011**, *13*, 10036–10047.

(37) Ganesan, V.; Madrid, E.; Malpass-Evans, R.; Carta, M.; McKeown, N.B.; Marken, F. Biphasic Voltammetry and Spectroelectrochemistry in Polymer of Intrinsic Microporosity-4-(3-Phenylpropyl)-Pyridine Organogel/Aqueous Electrolyte Systems: Reactivity of MnPc versus MnTPP. *Electrocatalysis* **2019**, *10*, 295–304.

(38) Ponomarev, I.I.; Skupov, K.M.; Ponomarev, Iv.I.; Razorenov, D.Y.; Volkova, Y.A.; Basub, V.G.; Zhigalina, O.M.; Bukalov, S.S.; Volfkovich, Y.M.; Sosenkin, V.E. New Gas-Diffusion Electrode Based on Heterocyclic Microporous Polymer PIM-1 for High-Temperature Polymer Electrolyte Membrane Fuel Cell. *Russ. J. Electrochem.* **2019**, *55*, 552–557.

(39) Skupov, K.M.; Ponomarev, I.I.; Volfkovich, Y.M.; Sosenkin, V.E.; Ponomarev, Iv.I.; Volkova, Y.A.; Razorenov, D.Y.; Buyanovskaya, A.G.; Talanova, V.N. Porous Structure Optimization of Electrospun Carbon Materials. *Russ. Chem. Bull.* **2020**, *69*, 1106–1113.

(40) Marken, F.; Madrid, E.; Zhao, Y.Z.; Carta, M.; McKeown, N.B. Polymers of Intrinsic Microporosity in Triphasic Electrochemistry: Perspectives. *ChemElectroChem* **2019**, *6*, 4332–4342.

(41) Madrid, E.; Lowe, J.P.; Msayib, K.J.; McKeown, N.B.; Song, Q.L.; Attard, G.A.; Düren, T.; Marken, F. Triphasic Nature of Polymers of Intrinsic Microporosity Induces Storage and Catalysis Effects in Hydrogen and Oxygen Reactivity at Electrode Surfaces. *ChemElectroChem* **2019**, *6*, 252–259.

(42) Weber, J.; Wain, A.J.; Attard, G.A.; Marken, F. Electrothermal Annealing of Catalytic Platinum Microwire Electrodes: Towards Membrane-Free pH 7 Glucose Micro-Fuel Cells. *Electroanalysis* **2017**, *29*, 38–44.

(43) Mahajan, A.; Bhattacharya, S.K.; Rochat, S.; Burrows, A.D.; Fletcher, P.J.; Rong, Y.Y.; Dalton, A.B.; McKeown, N.B.; Marken, F. Polymer of Intrinsic Microporosity (PIM-7) Coating Affects Triphasic Palladium Electrocatalysis. *ChemElectroChem* **2019**, *6*, 4307–4317.

(44) Leong, S.X.; Carta, M.; Malpass-Evans, R.; McKeown, N.B.; Madrid, E.; Marken, F. One-step Preparation of Microporous Pd@cPIM Composite Catalyst Film for Triphasic Electrocatalysis. *Electrochem. Commun.* **2018**, *86*, 17–20.

(45) Adamik, R.K.; Hernandez-Ibanez, N.; Iniesta, J.; Edwards, J.K.; Howe, A.G.R.; Armstrong, R.D.; Taylor, S.H.; Roldan, A.; Rong, Y.Y.; Malpass-Evans, R.; Carta, M.; McKeown, N.B.; He, D.P.; Marken, F. Platinum Nanoparticle Inclusion into a Carbonized Polymer of Intrinsic Microporosity: Electrochemical Characteristics of a Catalyst for Electroless Hydrogen Peroxide Production. *Nanomaterials* **2018**, *8*, 542.

(46) Fan, B.B.; Zhao, Y.Z.; Putra, B.R.; Harito, C.; Bavykin, D.; Walsh, F.C.; Carta, M.; Malpass-Evans, R.; McKeown, N.B.; Marken, F. Photoelectroanalytical Oxygen Detection with Titanate Nanosheet - Platinum Hybrids Immobilised into a Polymer of Intrinsic Microporosity (PIM-1). *Electroanalysis* **2020**, https://doi.org/10.1002/elan.202060353.

(47) Hao, L.; Liao, K.S.; Chung, T.S. Photo-Oxidative PIM-1 Based Mixed Matrix Membranes with Superior Gas Separation Performance. *J. Mater. Chem. A* **2015**, *3*, 17273–17281.

(48) Prasad, C.; Tang, H.; Liu, Q.Q.; Bahadur, I.; Karlapudi, S.; Jiang, Y.J. A Latest Overview on Photocatalytic Application of g-C_3N_4 Based Nanostructured Materials for Hydrogen Production. *Internat. J. Hydrogen Energy* **2020**, *45*, 337–379.

(49) Zhao, Y.Z.; Al Abass, N.A.; Malpass-Evans, R.; Carta, M.; McKeown, N.B.; Madrid, E.; Fletcher, P.J.; Marken, F. Photoelectrochemistry of Immobilised Pt@g-C_3N_4 Mediated by Hydrogen and Enhanced by a Polymer of Intrinsic Microporosity PIM-1. *Electrochem. Commun.* **2019**, *103*, 1–6.

(50) Zhao, Y.Z.; Dobson, J.; Harabajiu, C.; Madrid, E.; Kanyanee, T.; Lyall, C.; Reeksting, S.; Carta, M.; McKeown, N.B.; Torrente-Murciano, L.; Black, K.; Marken, F. Indirect Photo-Electrochemical Detection of Carbohydrates with Pt@g-C_3N_4 Immobilised into a Polymer of Intrinsic Microporosity (PIM-1) and Attached to a Palladium Hydrogen Capture Membrane. *Bioelectrochem.* **2020**, *134*, 107499.

(51) Qi, L.Y.; Shang, L.R.; Wu, K.; Qu, L.L.; Pei, H.; Li, W.; Zhang, L.X.; Wu, Z.W.; Zhou, H.H.; McKeown, N.B.; Zhang, W.X.; Yang, Z.J. An Interfacial Layer Based on Polymers of Intrinsic Microporosity to Suppress Dendrite Growth on Li Metal Anodes. *Chem. European J.* **2019**, *25*, 12052–12057.

(52) Hong, Z.J.; Ahmad, Z.; Viswanathan, V. Design Principles for Dendrite Suppression with Porous Polymer/Aqueous Solution Hybrid Electrolyte for Zn Metal Anodes. *ACS Energy Lett*. **2020**, *5*, 2466–2474.

(53) Li, C.Y.; Ward, A.L.; Doris, S.E.; Pascal, T.A.; Prendergast, D.; Helms, B.A. Polysulfide-Blocking Microporous Polymer Membrane Tailored for Hybrid Li-Sulfur Flow Batteries. *Nano Lett.* **2015**, *15*, 5724–5729.

(54) Gigli, M.; Kowalski, J.A.; Neyhouse, B.J.; D'Epifanio, A.; Brushett, F.R.; Licoccia, S. Investigating the Factors that Influence Resistance Rise of PIM-1 Membranes in Nonaqueous Electrolytes. *Electrochem. Commun.* **2019**, *107*, 106530.

(55) Hendriks, K.H.; Robinson, S.G.; Braten, M.N.; Sevov, C.S.; Helms, B.A.; Sigman, M.S.; Minteer, S.D.; Sanford, M.S. High-Performance Oligomeric Catholytes for Effective Macromolecular Separation in Nonaqueous Redox Flow Batteries. ACS Central Sci. 2018, 4, 189–196.

Insert Table of Contents artwork here